Numerical Simulation of Melting in Porous Media via an Interfacial Tracking Model

Qicheng Chen[*] and Mo Yang[†]
University of Shanghai for Science and Technology, Shanghai 200093, China

and

Yuwen Zhang[‡,§] and Ya-Ling He[**]
Xi'an Jiaotong University, Xi'an, Shaanxi 710049, China

Melting in porous media within a rectangular enclosure with presence of natural convection is simulated using an interfacial tracking method. This method combines the advantages of the both deforming and fixed grids methods. Convection in the liquid region is modeled using the Navier-Stokes equation with Darcy's term and Forchheimer's extension. The results obtained by using the interfacial tracking method validated by comparing with the existing experimental and numerical results. The results show that the interfacial tracing method is capable of solving natural convection controlled melting problems in porous media at both high and low Prandtl numbers.

Nomenclature

A	=	aspect ratio, W/H
c	=	specific heat (J/kg-K)
C_p	=	heat capacity (J/m^{3}K)
f_p	=	liquid fraction at grid point P
g	=	gravitational acceleration (m/s^2)
Gr	=	Grashof number, $g\beta\Delta T H^3 / v_\ell^2$
H	=	height of wall (m)
$h_{s\ell}$	=	latent heat of fusion (J/kg)
k_ℓ	=	thermal conductivity in the liquid (W/m-K)
K	=	dimensionless thermal conductivities, k/k_ℓ
$K_{s\ell}$	=	ratio of thermal conductivities, k_s / k_ℓ
$\hat{K}$	=	modified dimensionless thermal conductivity
Nu	=	Nusselt number at the heated wall, $Nu = hH/k_\ell$
p	=	pressure (Pa)
P	=	dimensionless pressure, $pH^2 / \rho v_I^2$
Pr	=	Prandtl number of the liquid PCM, v_ℓ / α_ℓ
Ra	=	Rayleigh number, Gr·Pr
s	=	location of solid-liquid interface (m)

[*] Graduate Student, College of Energy and Power Engineering.
[†] Professor and Associate Dean, College of Energy and Power Engineering.
[‡] Changjiang Scholar Guest Chair Professor, College of Energy and Power Engineering, Associate Fellow AIAA (Corresponding author). Email: zhangyu@missouri.edu
[§] Permanent address: Professor, Department of Mechanical and Aerospace Engineering, University of Missouri, Columbia, MO 65211, USA
[**] Professor and Director, Key Laboratory of Thermal Fluid Science and Engineering of MOE.

S	=	dimensionless location of solid-liquid interface, s/H
S^0	=	dimensionless location of solid-liquid interface at the last time step
Ste	=	Stefan number, $\text{Ste} = c_\ell(T_h - T_m)/h_{s\ell}$
t	=	time (s)
T	=	temperature (K)
u	=	velocity component in the x-direction (m/s)
U	=	dimensionless velocity in the x-direction, $U = uH/\nu_\ell$
u_I	=	solid-liquid interfacial velocity (m/s), $u_{I=} \ \partial s/\partial t$
U_I	=	dimensionless solid-liquid interfacial velocity, $u_I H/\nu_\ell$
v	=	velocity component in the y-direction (m/s)
V	=	dimensionless velocity in the y-direction, vH/ν_ℓ or volume (m^3)
W	=	width of the enclosure (m)
x	=	dimensional coordinate (m)
X	=	dimensionless coordinate, x/H
y	=	dimensional coordinate (m)
Y	=	dimensionless coordinate, y/H

Greek Symbols

α	=	thermal diffusivity (m^2/s)
ε	=	porosity
γ	=	liquid fraction in the equation (2)
δ	=	liquid fraction in the equation (3)
μ	=	viscosity of the liquid PCM (kg/ms)
ρ	=	density (kg/m^3)
v	=	kinematic viscosity (m^2/s)
κ	=	permeability (m^2)
Ω	=	heat capacity ratio, $\overline{\rho c}/(\rho c)_\ell$
θ	=	dimensionless temperature, $(T - T_m)/(T_h - T_m)$
τ	=	dimensionless time, $\nu_\ell t/H^2$

Subscripts

e	=	east face of the control volume
eff	=	effective
E	=	east
f	=	fluid
i	=	initial
ℓ	=	liquid
m	=	melting point
N	=	north
n	=	north face of the control volume
p	=	porous matrix
ref	=	reference
s	=	solid
S	=	south
w	=	west face of the control volume
W	=	west

I. Introduction

SOLID-liquid phase changes in porous media widely occur in various natural phenomena and industrial applications, including the freezing and melting of soils [1], artificial freezing of ground for mining and construction purposes [2], thermal energy storage [3], and freezing of soil around the heat exchanger coils of a ground based heat pump [4,5]. In the last several decades, quantitative experiments and numerical simulations were carried out by many researchers. Although the early studies about phase change in porous media treated melting and solidification as conduction controlled, the role and importance of natural convection is gradually recognized.

Since the location of the solid-liquid interface is unknown *a prior*, melting and solidification is referred as moving boundary problems. A variety of numerical techniques have been developed overcome the difficulties in handling moving boundaries: enthalpy method [6, 7], equivalent heat capacity method [8], isotherm migration method [9], and coordinate transformation method [10-15]. These methods have been introduced by researchers to. Some previous works on multidimensional moving boundary problems include Duda et al. [16], Saitoh [17], Gong and Mujumdar [18], Cao et al. [19], Khillarkar et al. [20], Chatterjee and Prasad [21] and Beckett et al. [22].

The above numerical models can be divided into two groups [23]: deforming grid schemes (or strong numerical solutions) and fixed grid schemes (or weak numerical solutions). Both groups could provide reasonably accurate results [24]. Two major methods in the fixed grid schemes are used to solve the phase change problems: the enthalpy method [25] and the equivalent heat capacity method [26, 27]. Cao and Faghri combined the advantages of enthalpy and equivalent heat capacity methods and proposed a temperature transforming model [28]. Zhang and Faghri used temperature transforming model to study phase change in a microencapsulated PCM [29] and an externally finned tube [30].

Beckermann and Viskanta [31] propose a generalized model based on volume-averaged governing equations for melting and solidification in porous media. Later, Chang and Yang [32] proved that Beckermann and Viskanta's model could handle even more complicated problems. Chakraborty and Dutta proposed a generalized formulation for evaluation of latent heat functions in enthalpy-based macroscopic models for the convection-diffusion phase change process [33]. Pal et al. carried out an enthalpy-based simulation for the evolution of equiaxial dendritic growth in an undercooled melt of a pure substance [34]. In addition to the aforementioned macroscopic models, Chatterjee and Chakraboty also developed an enthalpy-based lattice Boltzmann model for the diffusion dominated solid-liquid phase change [35]. DasGupta et al. proposed a homogenization-based upscaling as a superior technique over the conventional volume-averaging methodologies for effective property prediction in multiscale solidification melding [36].

Zhang and Chen proposed an interfacial tracking method to solve melting and resolidification of gold film subject to nano- to femtosecond laser heating [37]. Chen et al. successfully solved natural convection controlled melting in an enclosure at higher Rayleigh number by using the interfacial tracking method [38]. The interfacial tracking method combined the advantages of the deforming grid and fixed grid methods. The location of solid-liquid interface could be obtained by energy balance at solid-liquid interface at every time step. In this paper, the interfacial tracking method will be extended to solve melting in porous media within a rectangular enclosure with presence of natural convection. The results obtained by using the interfacial tracking method will be compared with the existing experimental and numerical results.

II. Physical Model

Figure 1 shows the physical model of the problem – melting in porous media within a rectangular enclosure. The top and bottom walls are insulated, whereas the left and right walls are kept at constant temperatures at T_h and T_c, respectively. The initial temperature is equal to T_i, which is below the melting point, T_m. The complicated interfacial geometries of the porous matrix and the solid and liquid phase prohibit a solution of the microscopic conservation equations for mass, momentum and energy. Therefore, some form of a macroscopic description of the transport processes must be employed. The porosity of the porous media is defined as
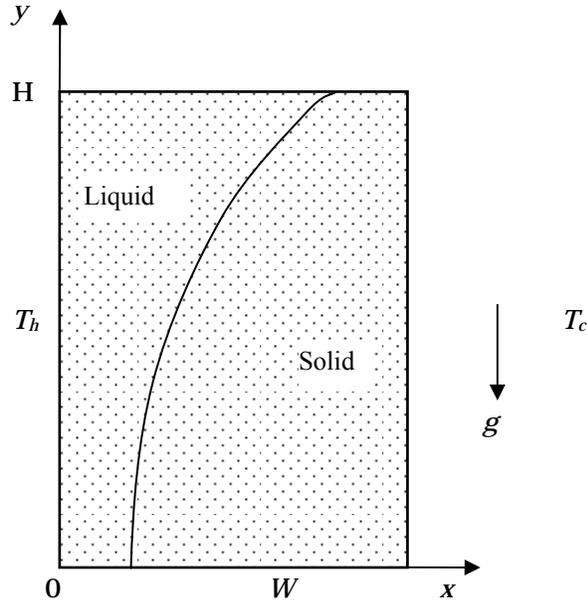
$$\varepsilon = \frac{V_f}{V} \tag{1}$$

Figure 1 Physical model

The liquid fraction in the pore space is defined as

$$\gamma(t) = \frac{V_\ell(t)}{V_f} \tag{2}$$

The volume fraction of liquid in the porous media is related to the porosity and liquid fraction:

$$\delta_\ell(t) = \frac{V_\ell(t)}{V} = \varepsilon\gamma(t) \tag{3}$$

The following assumptions are made:
1. The flow and heat transfer are two-dimensional and laminar.
2. The thermophysical properties of the porous matrix and the PCM are homogeneous and isotropic.
3. The porous matrix and PCM are in local thermal equilibrium.
4. The porous matrix and the solid phase of PCM are rigid (i.e. $\mathbf{u}_p = \mathbf{u}_s = 0$).
5. The porous matrix/fluid mixture is incompressible and the Boussinesq approximation can be invoked.
6. The thermophysical properties are constants, but are different for the porous matrix (p), liquid (l) and solid (s) phases.
7. The density change during phase change is neglected (i.e. $\rho_l = \rho_s = \rho_f$).

The dimensional governing equations are as following:

Continuity equation:

$$\frac{\partial u_\ell}{\partial x} + \frac{\partial v_\ell}{\partial y} = 0 \tag{4}$$

Momentum equation:

$$\frac{\rho_\ell}{\delta_\ell}\frac{\partial u_\ell}{\partial t} + \frac{\rho_\ell}{\delta_\ell^2}\left(u_\ell\frac{\partial u_\ell}{\partial x} + v_\ell\frac{\partial u_\ell}{\partial y}\right) = -\frac{\partial p}{\partial x} + \frac{\mu_\ell}{\delta_\ell}\left(\frac{\partial^2 u_\ell}{\partial x^2} + \frac{\partial^2 u_\ell}{\partial y^2}\right) - u_\ell\left(\frac{\mu_\ell}{\kappa} + \frac{\rho C}{\sqrt{\kappa}}\left(u_\ell^2 + v_\ell^2\right)^{\frac{1}{2}}\right) \tag{5}$$

$$\frac{\rho_\ell}{\delta_\ell}\frac{\partial v_\ell}{\partial t} + \frac{\rho_\ell}{\delta_\ell^2}\left(u_\ell \frac{\partial v_\ell}{\partial x} + v_\ell \frac{\partial v_\ell}{\partial y}\right) = -\frac{\partial p}{\partial y} + \frac{\mu_\ell}{\delta_\ell}\left(\frac{\partial^2 v_\ell}{\partial x^2} + \frac{\partial^2 v_\ell}{\partial y^2}\right) - v_\ell\left(\frac{\mu_\ell}{\kappa} + \frac{\rho C}{\sqrt{\kappa}}\left(u_\ell^2 + v_\ell^2\right)^{\frac{1}{2}}\right) - \rho g \beta\left(T - T_{ref}\right) \tag{6}$$

where u_ℓ and v_ℓ are the intrinsic phase averaged velocity of the liquid. The first- and second-order drag forces, named Dracy's term and Forchheimer's extension, are incorporated into Eqs. (5) and (6). Unlike Darcy's law that is valid for low flow velocity only, the momentum equations (5) and (6) with Forchheimer term included is applicable to wide range of flow velocities, including low and high flow velocities.

The Boussinesq approximation is represented by the last term of Eq. (6). The superficial velocity is related to the pore velocity by

$$u = \delta_\ell u_\ell, \quad v = \delta_\ell v_\ell \tag{7}$$

The permeability can be calculated from the Kozeny-Carman equation [39]

$$\kappa(\delta_\ell) = \frac{d_m^2 \delta_\ell}{175\left(1 - \delta_\ell\right)^2} \tag{8}$$

where d_m is the mean diameter of the particles. The value of the coefficient C in Forchheimer's extension has been measured experimentally by Ward [40], which was found to be 0.55 for many kinds of porous media.

Energy equation:

$$\overline{\rho c}\frac{\partial T}{\partial \tau} + \rho c_\ell\left(u \frac{\partial T}{\partial x} + v \frac{\partial T}{\partial y}\right) = \frac{\partial}{\partial x}\left(k_{eff}\frac{\partial T}{\partial x}\right) + \frac{\partial}{\partial y}\left(k_{eff}\frac{\partial T}{\partial y}\right) \tag{9}$$

where $\overline{\rho c}$ is the mean thermal capacitance of the mixture:

$$\overline{\rho c} = \varepsilon \rho_f\left[\gamma c_\ell + (1 - \gamma)c_s\right] + (1 - \varepsilon)\rho_p c_p \tag{10}$$

It should be noted that in the liquid region, $\gamma = 1$ and $\delta = \varepsilon$. On the other hand, in the pure solid region, both γ and δ are zero.

The effective thermal conductivity, k_{eff}, depends on the structure of the porous media. Veinberg [41] proposed a non-linear equation which he claimed to be universally applicable for a media with randomly distributed spherical inclusions

$$k_{eff} + \varepsilon\left[\frac{k_p - k_f}{k_f^{1/3}}\right]k_{eff}^{1/3} - k_p = 0 \tag{11}$$

where

$$k_f = \gamma k_\ell + (1 - \gamma)k_s \tag{12}$$

is the thermal conductivity of the PCM.

The boundary conditions of Eqs. (4) – (6) and (9) are:

Left vertical wall:

$$x = 0, T = T_h, u_\ell = 0, v_\ell = 0 \tag{13}$$

Right vertical wall:

$$x = W, T = T_c, u_\ell = 0, v_\ell = 0 \tag{14}$$

Bottom horizontal wall:

$$y = 0, \frac{\partial T}{\partial y} = 0, u_\ell = 0, v_\ell = 0 \tag{15}$$

Top horizontal wall:

$$y = H, \frac{\partial T}{\partial y} = 0, u_\ell = 0, v_\ell = 0 \tag{16}$$

Melting front:

$$x = s, \ T = T_m \tag{17}$$

$$x = s, \ \left[1 + \left(\frac{\partial s}{\partial y} \right)^2 \right] \left[k_{\ell,eff} \frac{\partial T_\ell}{\partial x} - k_{s,eff} \frac{\partial T_s}{\partial x} \right] = \delta_\ell \rho_\ell h_{s\ell} \frac{\partial s}{\partial t} \tag{18}$$

Introducing these following non-dimensional variables:

$$X = \frac{x}{H}, \ Y = \frac{y}{H}, \ S = \frac{s}{H}, \ U_\ell = u_\ell \frac{H}{\nu_\ell}, \ V_\ell = v_\ell \frac{H}{\nu_\ell}, \ \mathrm{P} = \frac{pH^2}{\rho \nu_\ell^2}, \tau = t \frac{\nu_\ell}{H^2}, \theta = \frac{T - T_m}{T_h - T_m}$$

$$K_{\ell,eff} = \frac{k_{\ell,eff}}{k_\ell}, K_{s,eff} = \frac{k_{s,eff}}{k_\ell}, \mathrm{Ste} = \frac{c_\ell(T_h - T_m)}{h_{s\ell}}, \ Sc = \frac{T_c - T_m}{T_h - T_c}, Da = \frac{\kappa(\varepsilon)}{H^2}, \Omega = \frac{\overline{\rho c}}{(\rho c)_\ell} \tag{19}$$

The governing equations can be non-dimensionalized as:

$$\frac{\partial U_\ell}{\partial X} + \frac{\partial V_\ell}{\partial Y} = 0 \tag{20}$$

$$\left[\frac{1}{\delta} \frac{\partial U_\ell}{\partial \tau} + \frac{1}{\delta^2} \left(U_\ell \frac{\partial U_\ell}{\partial X} + V_\ell \frac{\partial U_\ell}{\partial Y} \right) \right] = \frac{1}{\delta} \left(\frac{\partial^2 U_\ell}{\partial X^2} + \frac{\partial^2 U_\ell}{\partial Y^2} \right) - U_\ell \left(\frac{\kappa}{Da} + \frac{\kappa^{1/2} C}{Da^{1/2}} \left(U_\ell^2 + V_\ell^2 \right)^{\frac{1}{2}} \right) \tag{21}$$

$$\left[\frac{1}{\delta} \frac{\partial V_\ell}{\partial \tau} + \frac{1}{\delta^2} \left(U_\ell \frac{\partial V_\ell}{\partial X} + V_\ell \frac{\partial V_\ell}{\partial Y} \right) \right] = \frac{1}{\delta} \left(\frac{\partial^2 V_\ell}{\partial X^2} + \frac{\partial^2 V_\ell}{\partial Y^2} \right) - V_\ell \left(\frac{\kappa}{Da} + \frac{\kappa^{1/2} C}{Da^{1/2}} \left(U_\ell^2 + V_\ell^2 \right)^{\frac{1}{2}} \right) + Gr\theta \tag{22}$$

$$\Omega \frac{\partial \theta}{\partial \tau} + U_\ell \frac{\partial \theta}{\partial X} + V_\ell \frac{\partial \theta}{\partial Y} = \frac{K_{eff}}{\mathrm{Pr}} \left(\frac{\partial^2 \theta}{\partial X^2} + \frac{\partial^2 \theta}{\partial Y^2} \right) \tag{23}$$

where Gr is Grashof number based on the height of the enclosure.

$$Gr = g\beta \Delta T H^3 / \nu^2$$

The non-dimensional boundary conditions of Eqs. (20) – (23) are:

$$X = 0, \theta = 1, \ U_\ell = 0, V_\ell = 0 \tag{24}$$

$$X = 0, \theta = -Sc, \ U_\ell = 0, V_\ell = 0 \tag{25}$$

$$Y = 0, \frac{\partial \theta}{\partial Y} = 0, \ U_\ell = 0, V_\ell = 0 \tag{26}$$

$$Y = 1, \frac{\partial \theta}{\partial Y} = 0, \ U_\ell = 0, V_\ell = 0 \tag{27}$$

$$X = S, \theta = 0 \tag{28}$$

$$\frac{\delta_\ell}{K_{\ell,eff}} \frac{\mathrm{Ste}}{\mathrm{Pr}} \left[1 + \left(\frac{\partial S}{\partial Y} \right)^2 \right] \left[\frac{\partial \theta_\ell}{\partial X} - \frac{K_{s,eff}}{K_{\ell,eff}} \frac{\partial \theta_s}{\partial X} \right] = U_I \tag{29}$$

III. Numerical Procedures and Method

A. Discretization of Governing Equations

The above two-dimensional governing equations are discretized by using a finite volume method [42]. The conservation laws are applied over finite-sized control volume around grid points and the governing equations are then integrated over the control volume. Staggered grid arrangement is used in the discretization of the computational domain in the momentum equations. A power law scheme is used to discretize convection/diffusion terms in the momentum and energy equations. The algebraic equation resulting from this control volume approach is in the form of:

$$a_P \phi_P = \sum a_{nb} \phi_{nb} + b \qquad (30)$$

where ϕ_P represents the value of general variable ϕ (U, V or θ) at the grid point P, ϕ_{nb} are the values of the variable at P's neighbor grid points, and a_P, a_{nb} and b are corresponding coefficients and terms derived from original governing equations. The numerical simulation is accomplished by using SIMPLE algorithm [42]. The velocity-correction equations for corrected U and V in the algorithm are:

$$U_e = U_e^* + d_e(P_P^{'} - P_E^{'}) \qquad (31)$$

$$V_n = V_n^* + d_n(P_P^{'} - P_N^{'}) \qquad (32)$$

where e and n represent the control-volume faces between grid P and its east neighbor E and grid P and its north neighbor N, respectively. In this work, the governing equations are used for the entire computational domains. The velocity in the solid region is set to zero by letting $a_p = 10^{20}$ and b = 0 in the eq. (30) for the momentum equation.

B. Interfacial Tracking Method

Wang and Matthys [43] proposed an effective interface-tracking method by introducing an addition node at the interface, which divides the control volume containing interface into two small control volumes. In this work, an interfacial tracking method [37] that was developed for conduction controlled melting of metal film under irradiation of femtosecond laser will be extended to be able to handle convection-controlled solid-liquid phase change problem. This method is an alternative approach that does not require dividing the control volume containing interface but can still accurately account for energy balance at the interface. For the control volume that contains a solid-liquid interface, the dimensionless temperature θ_P is numerically set as interfacial temperature ($\theta_I = 0$) by letting

$a_P = 10^{20}$ and $b = 0$ in the eq. (30) with $\phi = \theta$.

The above treatment yields an accurate result when the solid-liquid interface is exactly at grid point P, there are two scenarios as shown in Fig. 2 (b): as shown in Fig. 2 (a). When the interfacial location within the control volume is not at grid point P, the interface is on the right side of the grid point, or (c) the interface is on the left side of the grid point.

With the scenarios (b) and (c), a modified dimensionless thermal conductivity, $\hat{K}_w$, at the face of the control volume w is introduced by equating the actual heat flux across the face of the control volume w, based on the position and temperature of the main grid point, P [44],

$$\frac{K_w(\theta_W - \theta_I)}{(\delta X)_w + (f_P - 0.5)(\Delta X)_P} = \frac{\hat{K}_w(\theta_W - \theta_P)}{(\delta X)_w} \tag{33}$$

Considering $\theta_P = \theta_I$, eq. (33) becomes

$$\hat{K}_w = \frac{(\delta X)_w}{(\delta X)_w - (0.5 - f_P)(\Delta X)_P} K_w \tag{34}$$

Similarly, a modified thermal conductivity at face e of the control volume can be obtained as

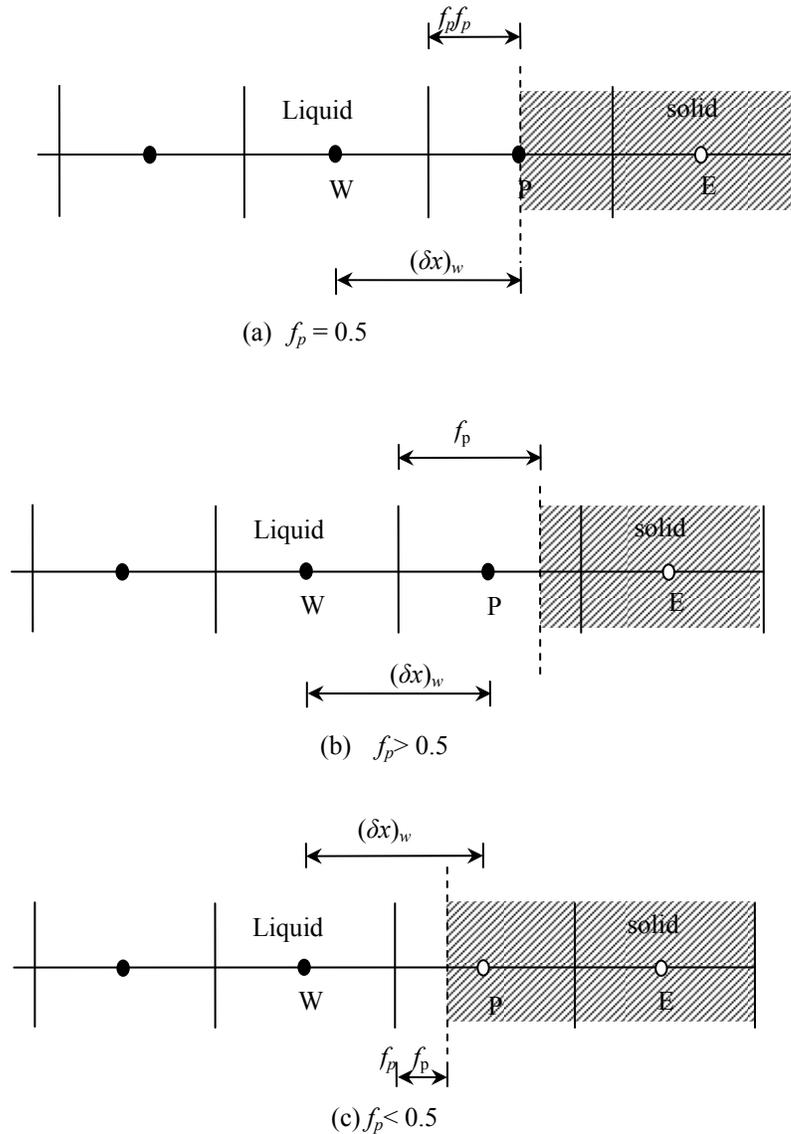$$\hat{K}_e = \frac{(\delta X)_e}{(\delta X)_e + (0.5 - f_P)(\Delta X)_P} K_e \tag{35}$$

(a) $f_p = 0.5$

(b) $f_p > 0.5$

(c) $f_p < 0.5$

Figure 2 Grid systems near the liquid-solid interface

The modified thermal conductivities defined by eqs. (34) and (35) are used to obtain the coefficients for grid points W and E, which allows the temperature at the main grid, P, to be used in the computation regardless of the location of the interface within the control volume. To determine the interfacial location, the energy balance at the interface, eq. (29) can be discretized and the solid-liquid interfacial velocity can be obtained as

$$U_I = \frac{Ste}{\Pr}\left[1+\left(\frac{S-S_S}{(\delta Y)_s}\right)^2\right]\left[\frac{K_w(\theta_W - \theta_I)}{(\delta X)_w - (0.5 - f_P)(\Delta X)_P} - \frac{K_e(\theta_I - \theta_E)}{(\delta X)_e + (0.5 - f_P)(\Delta X)_P}\right] \quad (36)$$

where S_S is the interfacial location at the grid at the south of grid P.

The interfacial location is then determined using

$$S = S^0 + U_I \Delta \tau \quad (37)$$

and the liquid fraction in the control volume that contain interface is

$$f = \frac{S - X_P - (\Delta X)_P / 2}{(\Delta X)_P} \quad (38)$$

C. Numerical Solution Procedure

The numerical solution starts from time $\tau = 0$. Once the temperature at the first control volume from the heated surface obtained exceeds the melting point, the temperature of the first control volume sets at the melting point by letting $a_P = 10^{20}$ and $b = 0$ in the Eq. (29) with $\phi = \theta$. After melting is initiated, the following iterative procedure is employed to solve for the interfacial velocity and the interfacial location at each time step:

  (1) Assume an interface velocity U_I, using the velocity U_I of last time step as initial value.

  (2) Determine the new interface location, S, from eq. (37).

  (3) Obtain the modified dimensionless thermal conductivity, $\hat{K}_w$ and $\hat{K}_e$, at the faces of the control volume w and e from eqs. (34) and (35).

  (4) Solve eqs. (20)- (23) to obtain the temperature distributions and obtain the new interface velocity U_I by using eq. (36).

  (5) Compare the newly obtained U_I and the assumed value in Step 1. If the difference is less than 10^{-5} and the maximum difference between the temperatures obtained from two consecutive iterative steps is less than 10^{-5}, the interfacial location for the current step is obtained. If not, the process is repeated until the convergence criterion is satisfied. To obtain converged solution of flow field, under-relaxation was employed for velocity and pressure and the under-relaxation factors for velocity and pressures are 0.5 and 0.8, respectively.

The interfacial tracking method developed in this paper eliminated the needs for of assuming the range of phase change temperature in other fixed grid methods like equivalent heat capacity method or temperature transforming model. It does not product nonlinear oscillation on the temperature and interfacial location like enthalpy and equivalent heat capacity methods.

IV. Results and discussion

The interfacial tracking method will be validated by comparing its results with experimental results as well as other numerical results. The numerical simulation of melting of gallium saturated in packed glass bead is performed first

under the conditions that are same as the experiments carried out by Becermann and Viskanta [31]. The top and bottom walls were constructed of phenolic plates, while the vertical front and back walls were made of Plexiglass. The two vertical sidewalls, which served as the heat source or sink, were multi-pass heat exchangers machined out of a copper plate. The heat exchangers were connected through a valve system to two constant temperature baths. Through an appropriate valve setting the vertical sidewalls could be maintained at a constant temperature. The left wall is kept at high constants dimensionless temperature of T_h=0.6, and low constant dimensionless temperature equal to the subcooling parameter, Sc=0.4. The Rayleigh number is 8.409×10^5, the Stefan number is 0.1241, the Prandtl number is 0.0208, the Darcy number is 1.37×10^{-5}, A=1.0, the heat capacity ratios in liquid and solid are Ω=0.864 and 0.8352, respectively. The dimensionless thermal conductivities are used the same value in the liquid and solid phases, K_{eff}=0.27. After grid number and time step test, the grid number used in the simulation was 40×40 and the dimensionless time step was 2×10^{-5}. Figure 3 shows the positions of melting fronts obtained by interfacial tracking method compared with experimental by Beckermann and Viskanta [31] at different dimensionless times. At the early time, the present melting interfacial velocity is faster than the experimental result near the top of the enclosure; however, the melting interfacial velocity obtained by the interfacial tracking method is closer to the numerical results obtained by Beckermann and Viskanta [31]. The melting front is almost parallel to the heated wall, which indicates that the process is dominated by conduction at the early stage. As time progressing, the melting front gradually exhibits shapes that are typical for convection-controlled melting process. At later time, the interface becomes more inclined as the melting continues toward a steady state, whereas a good agreement between the numerical and experimental results can also be observed. At a longer time of τ=0.152, the interfacial tracking method gives result very close to the experimental results and numerical results. The difference between the predicted and measured interface position is less than 1%.
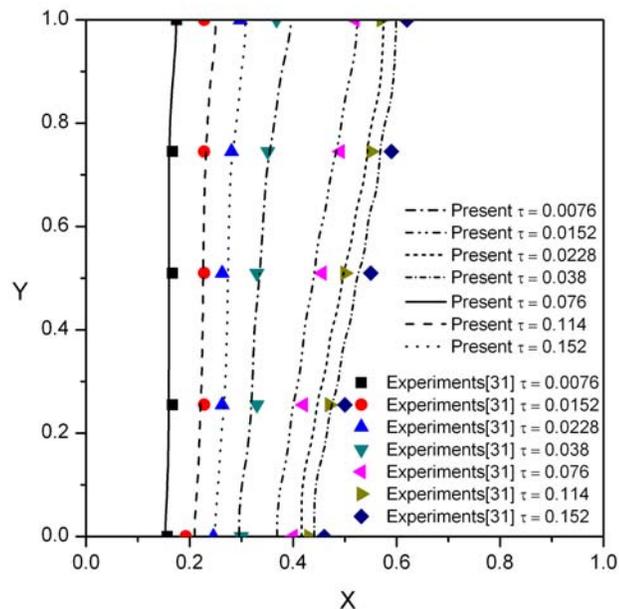

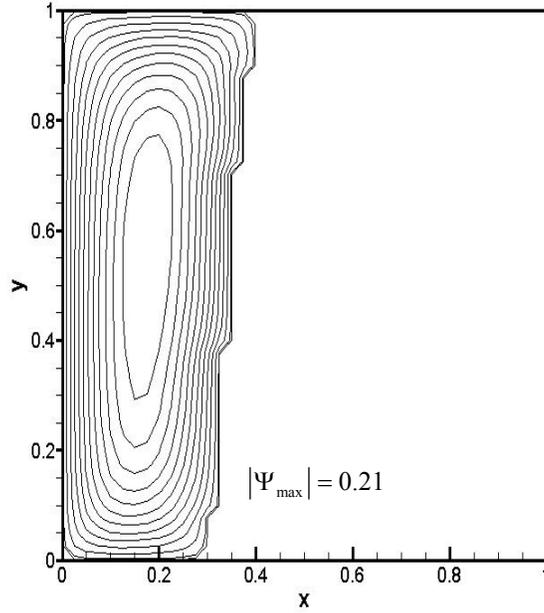**Figure 3 Comparison of the locations of the melting fronts (Ra =8.04×10^5, Pr=0.0208)**

Figure 4 Streamlines at τ = 0.0038 (Ra =8.04×10⁵, Pr=0.0208)

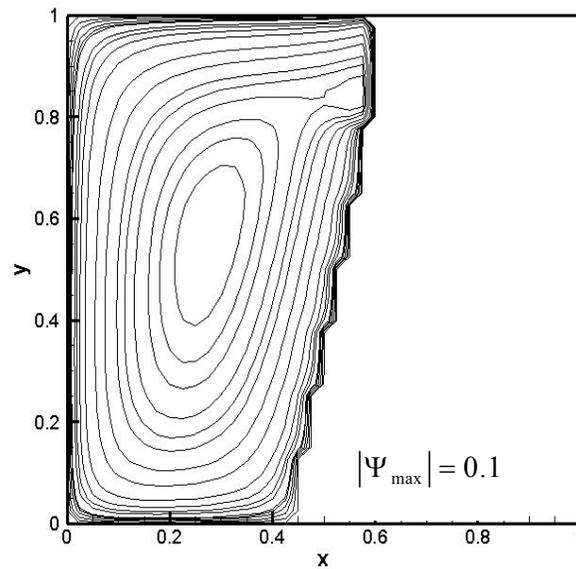**Figure 5 Streamlines at τ = 0.152 (Ra =8.04×10⁵, Pr=0.0208)**

Figures 4 and 5 show the streamlines at different dimensionless times of $\tau = 0.038$ and $\tau = 0.152$, respectively. The streamlines at $\tau = 0.038$ shown in Fig. 4 indicate that the liquid is heated by the left wall and rises toward the top wall, which causes fast melting of the top portion of the PCM. When dimensionless time $\tau = 0.152$, the melting process nearly reached to steady-state, shown in Fig. 5.

Figures 6 and 7 show the temperature profiles at different heights in the enclosure. As shown in Fig. 6, the temperature profiles at different heights are very closer to each other at early time of $\tau = 0.038$, because the melting is driven by conduction in the liquid region. At dimensionless time $\tau = 0.152$, shown in Fig. 7, the temperature

profiles at different heights become very different from each other because the effect of convection becomes stronger as time progresses. The convection causes the temperature of top point much higher than that of bottom point. Figures 6 and 7 reveal the excellent agreement between the results from the interfacial tracking method and the results from the Beckermann and Viskanta's numerical simulation [31]. The difference between the temperatures obtained by the present paper and Ref. [31] is less than 1% at any point and any time.

The above comparisons show that the present method of the phase-change process is well suited for simulating melting in a porous medium.
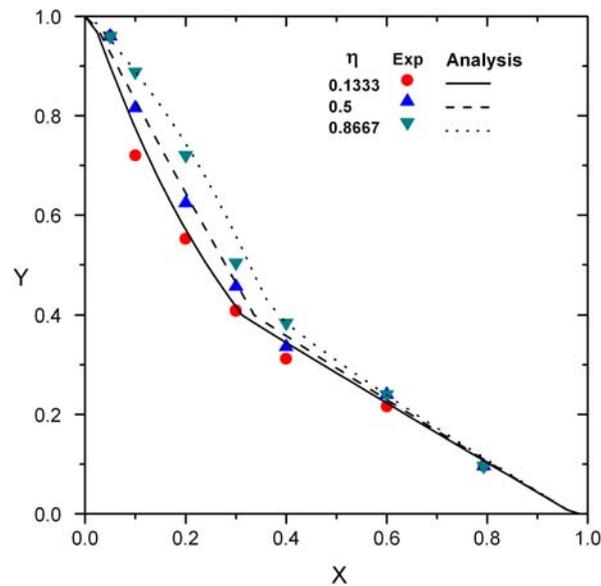

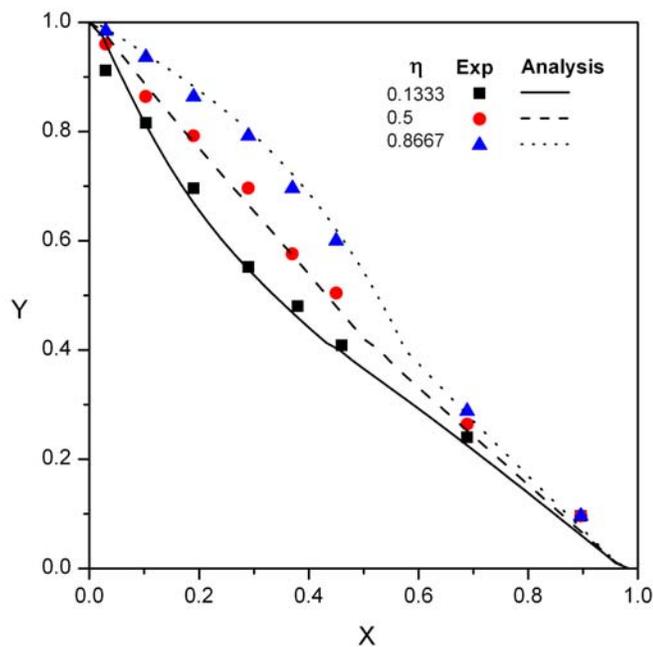**Figure 6 Temperature profiles at $\tau = 0.0038$ (Ra $=8.04\times10^5$, Pr=0.0208)**

Figure 7 Temperature profiles at $\tau = 0.152$ (Ra $=8.04\times10^5$, Pr=0.0208)

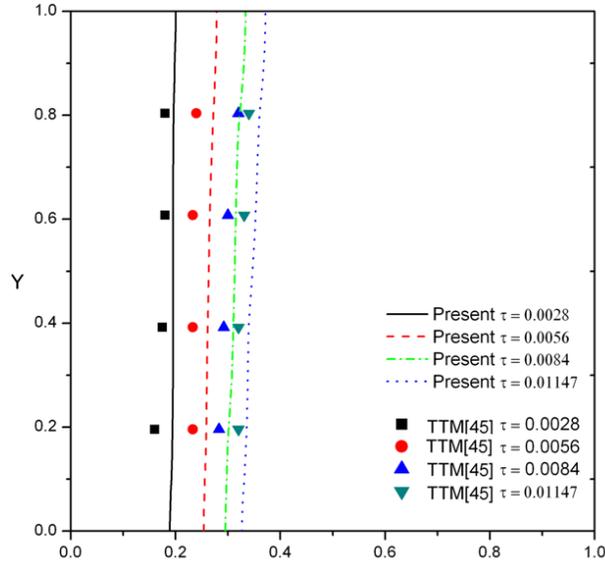**Figure 8 Comparison of the locations of the melting fronts (Ra =1.26×10^6, Pr=1.55×10^{-3})**

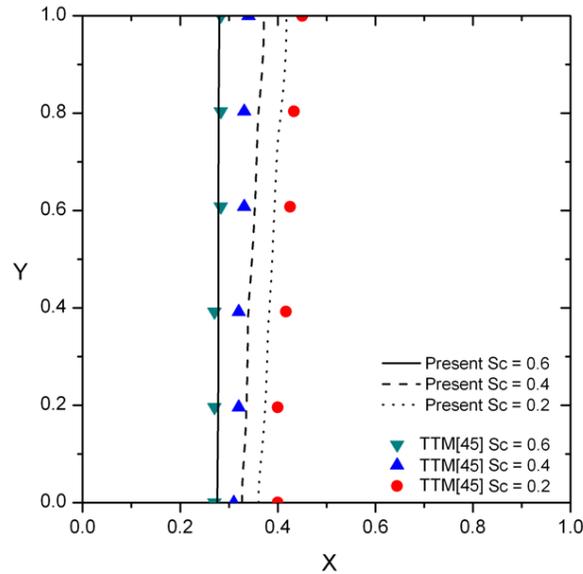**Figure 9 Effects of the subcooling number on the melting process (Ra =1.26×10^6, Pr=1.55×10^{-3})**

In order to make sure that the interfacial tracking method is also valid at low Prandtl number in a porous medium, an additional numerical simulation was performed based on the conditions specified by Damronglerd and Zhang [45]. The aspect ratio of the enclosure is A = 1. The subcooling parameter is equal to 0.4, the Rayleigh number is 1.28×10^6, the Stefan number is 0.0295, the Prandtl number is 1.55×10^{-3}, $K_{s,eff}$ is 0.414, $K_{l,eff}$ is 0.402, and ε is 0.385. After grid number test, the grid number used in the simulation was 40×40，and the time step was 2×10^{-6}.

Figure 8 shows the comparison between the locations of solid-liquid interfaces obtained by using the present model and the temperature transforming model (TTM) used by Damronglerd and Zhang [45]. At early dimensionless time of τ=0.0028, the agreement is very good at the bottom and top regions of the rectangular cavity. Since the Prandtl number is very low, the heat transfer in the whole liquid region is govern by conduction. As melting continues to the dimensionless time of τ=0.0056, the effect of the nature convection makes the top portion

of the liquid region wider. When the dimensionless time τ=0.01147, the effect of nature convection on the melting became stronger than any previous times. Figure 9 shows a comparison of the influence on the subcooling number on the melting process. The Results show that the melting front moves faster at the low subcooling parameter, *Sc*=0.2, and slower at the high subcooling parameter, *Sc*=0.6.

Comparisons between all the numerical results obtained by interfacial tracking method and obtained by the modified temperature transforming model indicate that the largest difference is only 0.16%. Therefore, the interfacial tracking method also can obtain very good results even at lower Prandlt number during natural convection controlled melting in porous media.

V. Conclusions

An interfacial tracking method for two dimensional convection-controlled melting problems in porous media was developed. It eliminated the needs for of assuming the range of phase change temperature in other fixed grid methods. It does not product nonlinear oscillation on the temperature and interfacial location like enthalpy and equivalent heat capacity methods. Comparison between the results obtained by the present interfacial tracking method and Beckermann and Viskanta's enthalpy method and Damronglerd and Zhang's TTM shows that the interfacial tracking method could be used to solve the solid-liquid phase change in porous media in wide ranges of Rayleigh and Prandtl numbers.

Acknowledgement

References

[1] Miller, R, D., "Freezing Phenomena in Soils," Applications of Soil Physics, 1980, pp. 254-318. Academic Press, New York.

[2] Sanger, F. J., "Ground Freezing in Construction," ASCE Mech. Foundation Div. Vol. 94, 1968, pp. 131-158.

[3] ME Staff, "Seasonal Thermal Energy Storage," Mech. Eng, Vol. 155, 1983, pp. 28-34.

[4] Metz, P. D., "A Simple Computer Program to Model Three-Dimensional Underground Heat Flow with Realistic Boundary Conditions," ASME J. Solar Energy Vol. 105, 1983, pp. 42-49.

[5] Svec, O., Goodrish, L. E., and Planar, J. H. L., "Heat Transfer Characteristics of Inground Heat Exchange," J. Energy Res. Vol. 7, 1983, pp. 263-278.

[6] Shamsundar, N., and Sparrow, E.M., "Effect of Density Change on Multidimensional Conduction Phase Change," Journal of Heat Transfer, Vol. 98, 1976, 550-557.

[7] Crowley, A.B., "Numerical Solution of Stefan Problems," International Journal of Heat and Mass Transfer, Vol. 21, 1978, pp. 215-219.

[8] Bonacina, C., Comini, G., Fasano, A., Primicerio, M., "Numerical Solution of Phase-Change Problems," International Journal of Heat and Mass Transfer, Vol. 16, 1973, 1825-1832.

[9] Crank, J., and Gupta, R.S., "Isotherm Migration Method in Two Dimensions," International Journal of Heat and Mass Transfer, Vol. 18, 1975, pp. 1101-1107.

[10] Hsu, C.F., Sparrow, E.M., Patankar, S.V., "Numerical Solution of Moving Boundary Problems by Boundary Immobilization and a Control-Volume Based Finite Difference Scheme," International Journal of Heat and Mass Transfer, Vol. 24, 1981, 1335-1343.

[11] Sparrow, E.M., Chuck, W., "An Implicit/explicit Numerical Solution Scheme for Phase-Change Problems," Numerical Heat Transfer, Vol. 7, 1984, pp. 1-15.

[12] Sparrow, E.M., Ramadhyani, S., Patankar, S.V., "Effect of Subcooling on Cylindrical Melting," Journal of Heat Transfer, Vol. 100, 1978, 395-402.

[13] Cheung, F.B., Chawla, T.C., Pedersen, D.R., "The Effect of Heat Generation and Wall Interaction on Freezing and Melting in a Finite Slab," International Journal of Heat and Mass Transfer, Vol. 27, 1984, pp. 29-37.

[14] Rattanadecho, P., "Experimental And Numerical Study Of Solidification Process In Unsaturated Granular Packed Bed," AIAA Journal of Thermophysics and Heat Transfer, Vol. 18, No. 1, 2004, pp. 87–93.

[15] Rattanadecho, P., "The Theoretical and Experimental Investigation of Microwave Thawing of Frozen Layer Using Microwave Oven (Effects of Layered Configurations and Layered Thickness)," International Journal of Heat and Mass Transfer, Vol. 47, No. 5, 2004, pp. 937–945.

[16] Duda, J.L., Malone, M.F., Notter, R.H., Vrentas, J.S., "Analysis of Two Dimensional Diffusion Controlled Moving Boundary Problems," International Journal of Heat and Mass Transfer, Vol. 18, 1975, pp. 901-910.

[17] Saitoh, T., "Numerical Method for Multi-Dimensional Freezing Problems in Arbitrary Domains," Journal of Heat Transfer, Vol. 100, 1978, pp. 294-299.

[18] Gong, Z.-X., Mujumdar, A.S., "Flow and Heat Transfer in Convection Dominated Melting in a Rectangular Cavity Heated From Below," International Journal of Heat and Mass Transfer, Vol. 41, No. 17, 1998, pp. 2573–2580.

[19] Cao, W., Huang, W., Russell, R.D., An r-adaptive Finite Element Method based upon Moving Mesh PDEs," Journal of Computational Physics, Vol. 149, 1999, pp. 221-244.

[20] Khillarkar, D.B., Gong, Z.X., Mujumdar, A.S., "Melting of a Phase Change Material in Concentric Horizontal Annuli of Arbitrary Cross-Section," Applied Thermal Engineering, Vol. 20, No. 10, 2000, pp. 893–912.

[21] Chatterjee, A., and Prasad, V., "A Full 3-Dimensional Adaptive Finite Volume Scheme for Transport and Phase-Change Processes Part I: Formulation and Validation," Numerical Heat Transfer; Part A: Applications, Vol. 37, No. 8, 2000, pp. 801–821.

[22] Beckett, G., MacKenzie, J.A., and Robertson, M.L., "A Moving Mesh Finite Element Method for the Solution of Two-Dimensional Stefan Problems," Journal of Computational Physics, Vol. 168, No. 2, 2001, 500–518.

[23] Voller, V. R., "An Overview of Numerical Methods for Solving Phase Change Problems," Advances in Numerical Heat Transfer, Vol. 1, W. J. Minkowycz and E. M. Sparrow, eds., Taylor & Francis, Basingestoke, 1997.

[24] Sasaguchi, K., Ishihara, A., and Zhang, H., Numerical Study on Utilization of Melting of Phase Change Material for Cooling of a Heated Surface at a Constant Rate, Number. Heat Transfer, Part A, Vol. 29, 1996, pp.19-31.

[25] Binet, B., and Lacroix, M., Melting From Heat Sources Flush Mounted on a Conducting Vertical Wall, Int. J. Numer. Methods Heat Fluid Flow, Vol. 10, 2000, pp. 286-306.

[26] Morgan, K., A Numerical Analysis of Freezing and Melting With Convection, Comput. Methods Appl. Mech. Eng., Vol. 28, 1981, pp.275-284.

[27] Hsiao, J. S., An Efficient Algorithm for Finite Difference Analysis of Heat Transfer With Melting and Solidification, ASME Paper No. 84-WA/HT-42, 1984.

[28] Cao, Y., and Faghri, A., A Numerical Analysis of Phase Change Problem Including Natural Convection, Journal of Heat Transfer, Vol. 112, No. 3, 1990, pp. 812-815.

[29] Zhang, Y. and Faghri, A., "Analysis of Forced Convection Heat Transfer in Microencapsulated Phase Change Material Supensions". Journal of Thermophysics and Heat Transfer, Vol. 9, No. 4, 1995, pp. 727-732.

[30] Zhang, Y. and Faghri, A., "Heat Transfer Enhancement in Latent Heat Thermal Energy Storage System by Using an External Radial Finned Tube". Journal of Enhanced Heat Transfer, Vol. 3, No. 4, 1996, pp. 119-127.

[31] Beckermann, C., and Viskanta, R., "Natural Convection Solid/Liquid Phase change in Porous Media", International Journal of Heat and Mass Transfer, Vol. 31, No.1, 1988, pp. 35-46.

[32] Chang, W. J., and Yang, D. F., "Natural Convection for the Melting of Ice in Porous media in a rectangular Enclosure," International Journal of Heat and Mass Transfer, Vol. 39, No. 11, 1996, pp. 2333-2348.

[33] Chakraborty, S., and Dutta, P., "A Generalized Formulation for Evaluation of Latent Heat Functions in Enthalpy-Based Macroscopic Models for Convection-Diffusion Phase Change Processes", Metallurgical and Materials Transactions B: Process MeTallurgy and Materials Processing Science, Vol. 32, No. 3, 2001, pp. 320-330

[34] Pal, D., Bhattacharya, J., Dutta, P., and Chakraborty, S., "An Enthalpy Model for Simulation of Dendritic Growth", Numerical Heat Transfer, Part B: Fundamentals, Vol. 50, No. 1, 2006, pp. 59-78.

[35] Chatterjee, D., and Chakraborty, S., "A Hybrid Lattice Boltamann Model for Solid-Liquid Phase Transition in Presence of Fluid Flow", Physics Letters A, Vol. 351, Nos. 4-5, 2006, pp.359-367.

[36] DasGupta, D., Basu, S., and Chakraboty, S., "Effective Propertty Predictions in Multi-Scale Solidification Modeling Using Homogenization Theory", Physics Letters A, Vol. 348, Nos. 3-6, 2006, pp. 386-396.

[37] Zhang, Y. and Chen, J.K., "An Interfacial Tracking Method for Ultrashort Pulse Laser Melting and Resolidification of a Thin Metal Film," Journal of Heat Transfer, Vol. 130, No. 6, 2008,   062401

[38] Chen, Q., Zhang, Y., and Yang, M., 2011, "An Interfacial Tracking Method for Natural Convection Controlled Melting in an Enclosure," *Numerical Heat Transfer*, Part B: Fundamentals, Vol. 59, No. 2, 2011, pp. 209-225.

[39] Faghri, A., and Zhang, Y., *Transport Phenomena in Multiphase Systems*, Elsevier, Burlington, MA, 2006.

[40] Gray, W. G., and O'Neill, K., "On the general Equations for flow in porous media and their reduction to Darcy's law, Water Resour. Res., Vol. 12, 1976, pp. 148-154.

[41] Veinberg, A. K., Permeability, electrical conductivity, dielectric constant and thermal conductivity of a medium with spherical and ellipsoidal inclusions, Soviet Phys, Dokl. Vol. 11, 1967, pp. 593-595.

[42] Pantankar, S. V., Numerical Heat Transfer and Fluid Flow, McGraw-Hill, New York, NY, 1980.

[43] Wang, G. X., and Matthys, E. F., Numerical Melting of Phase Change and Heat transfer During Rapid Solidification Processes: Use of Control Volume Integral with Element Subdivision, Int. J. heat Mass Transfer, Vol. 35, 1992, pp. 141-153.

[44] Olsson, E.D., and Bergman, T.L., Reduction of Numerical Fluctuations in Fixed Grid Solidification Simulations, AIAA/ASME Thermal Physics and Heat Transfer Conference, Seattle, WA, June 18-20, ASME HTD-Vol. 130, 1990, pp. 130-140.

[45] Damronglerd, P., and Zhang, Y., "Numerical Simulation of Melting in Porous Media via a Modified Temperature-Transforming Model", Journal of Thermophysics and Heat Transfer. Vol. 24, No. 2, 2010, pp. 340-347.